

Cite this: *Phys. Chem. Chem. Phys.*, 2012, **14**, 4142–4154

www.rsc.org/pccp

PAPER

Reaction network governing diphosphine-protected gold nanocluster formation from nascent cationic platforms†

John M. Pettibone^a and Jeffrey W. Hudgens^{*b}

Received 8th September 2011, Accepted 5th December 2011

DOI: 10.1039/c2cp22865c

We identify the reaction network governing gold monolayer protected cluster (MPC) formation during the reduction of Au(PPh₃)Cl and L⁵ (L⁵ = 1,5-bis(diphenylphosphino)pentane) in solutions. UV-vis spectroscopy and electrospray ionization mass spectrometry (ESI-MS) monitored the formation of ligated Au_x: 6 ≤ x ≤ 12 clusters, which comprise the reaction intermediates and final products. Initially, predominantly [Au₂L⁵₂]²⁺ complexes form through dissolution of Au(PPh₃)Cl. These complexes control the reduction and nucleation reactions that form nascent phosphine-ligated Au₈ and Au₁₀ ionic clusters. [Au₁₀L⁵₄]²⁺ is an observed growth platform for ligated Au₁₁ and Au₁₂ clusters. The data for syntheses of Au:L⁵ systems evidence that the nascent reaction products (*t* < 3 days) are less dependent on the chosen reducing agent (borane *tert*-butylamine complex or NaBH₄); instead, after reduction ceases, subsequent solution phase processing provides greater control for tuning cluster nuclearity.

Introduction

Significant work has been devoted to the development of phosphine protected gold nanoclusters of different nuclearity.^{1–9} The structures of these gold-PPh₃ and other gold-phosphine ligand complexes, derived from X-ray crystallographic, (³¹P ¹H) NMR and Mössbauer data, helped validate polyhedral skeletal electron pair (PSEP) theory.^{10–12} However, the gold reduction reaction typically yields a broad product distribution,^{13–15} such that subsequent purification is necessary to isolate desired products.^{6,16,17} The reduction of AuClPPh₃ is reported to be strongly controlled by kinetic parameters, similar to metal salt reduction.^{14,18} Reduction of salts and AuClPPh₃ can result in single product syntheses through application of post-reduction solution phase processing, *e.g.*, oxidation or subsequent reactant addition. These post-reduction solution phase processes have been successful at producing different gold nuclearity clusters, unique geometries, and distinct properties of usually the most stable clusters.^{11,19–23} Although these techniques have been successful, the controlling factors that narrow product distributions have not been elucidated. It is likely necessary to

identify the mechanism governing product formation in order to develop aimed approaches that lead to specific products. Detailed knowledge of the mechanism would promote significant advancement in rational synthesis design.

We have recently shown that phosphine ligands have the ability to both protect and proactively etch gold nanoclusters.¹⁴ The ability of phosphines to etch metal cores allows “size-selective processing” to occur around stable nanoclusters. Size-selective processing requires that competing reactions of growth and etching around stable clusters result in a progressively narrower product distribution. It is a post-reduction, solution phase processing phenomenon. However, the prerequisite for applying size-selective processing is knowledge of the relative reaction rates around specific clusters, resulting in desired product formation. Therefore, an outline of the reaction network that controls product formation for ligated metal nanoclusters of distinct stoichiometry would provide a roadmap for construction of aimed syntheses.

The gold-phosphine system (L^{*n*} = 1,*n*-bis(diphenylphosphino)alkane; Fig. 1), because it has shown the propensity to yield narrow product distributions.^{13,24} Thus, it is an ideal system for (partially) elucidating the reaction network controlling product formation. Recently, research on the gold-diphosphine systems has intensified. A computational study by Hong *et al.*²⁵ has examined overall nanocluster stability and selectivity with diphosphines containing spacers of different lengths. They reported that diphosphines, such as L³, can selectively stabilize clusters of specific gold nuclearity; however, they also concluded that the conditions that make selectivity possible are more complex than stabilization alone. Experimental results support their conclusion. For example,

^a Material Measurement Laboratory, National Institute of Standards and Technology, 100 Bureau Drive, MS-8320, Gaithersburg, MD 20899-8320, USA. E-mail: john.pettibone@nist.gov

^b Material Measurement Laboratory, National Institute of Standards and Technology, 100 Bureau Drive, MS-8362, Gaithersburg, MD 20899-8362, USA. E-mail: jeffrey.hudgens@nist.gov

† Electronic supplementary information (ESI) available: ESI-MS data for Au:L⁵ synthesis solutions involving neat (100%) chloroform, dynamic light scattering data, and a description of the role of oxidation on stability of complexes and cluster formation. See DOI: 10.1039/c2cp22865c

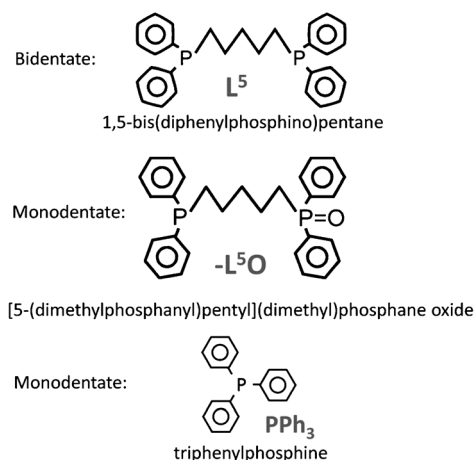


Fig. 1 Illustrations of the ligands, which are observed to form complexes with gold during this study.

ESI-MS data observed, as a 1 : 1 L^6 : Au(PPh₃)Cl solution is reduced by NaBH₄ initially ($t < 10$ min), exhibits ligated Au₈ and Au₁₀ clusters. Although reduction soon ceases, the solution continues to evolve. By $t = 6$ days the Au₁₀ signal is nil, and the solution exhibits only [Au₈L₆]²⁺, but by $t = 6$ days the solution exhibits mainly signal from [Au₉L₄Cl]²⁺ and trace abundances of Au₈ and Au₁₀ cations. As a second example, Shichibu and Konishi have reported that reduction of Au₂L₂Cl₂ in air initially forms a disperse distribution of cationic ligated clusters ranging from Au₉ to Au₁₅; but, after addition of HCl, the solution yields monodisperse [Au₁₃L₅Cl]³⁺.¹⁵ Interestingly, diphosphine ligands with different alkane chain links did not result in Au₁₃ clusters. Previously, van der Velden *et al.*²⁶ reported the synthesis of L¹-protected Au₁₃ clusters *via* reduction of [Au₂L₁]₂(NO₂)₂. Furthermore, etching of gold nanoclusters has also been promoted by halides and pseudohalides.²⁷ These different approaches result in narrow product distributions, but whether formation is through growth or degradation (etching) pathways is not established. Therefore, the major controlling factors for single product formation will continue to remain unidentified without an examination of the specific reactions governing formation.

For this study we have used electrospray mass spectrometry (ESI-MS) and UV-vis data to formulate a chemically-detailed reaction network governing the syntheses of Au : L⁵ clusters. The reaction network forms a basis for developing “size-selective” syntheses of Au_{*x*} : L⁵ nanoclusters. We find that the reaction pathways for Au : L⁵ clusters are built through stable Au₁₀ platforms with further cluster processing controlled by solution equilibria. We report syntheses of new phosphine-protected gold-centered Au₁₂ clusters. An important new insight into size-selective nanocluster syntheses is that nascent reaction products formed by the condensation of gold-phosphine complexes are relatively insensitive to the chosen reducing agent (*e.g.*, BTBC or NaBH₄); instead, after reduction processes cease, subsequent solution phase processing provides greater control for tuning cluster nuclearity.

The reaction network comprises the chemical reactions and associated rate coefficients that lead to products. Measurements of

initial reactants, chemical intermediates, and products reveal those reactions with finite rate coefficients as well as those with effectively null reaction rates. For this task we have adjusted synthesis conditions in the Au : L⁵ system to maximize the number of active formation pathways observable with ESI-MS and UV-vis methods. These results identify possible monodisperse products that may be achieved through optimization of synthesis conditions. System optimization to create monodisperse products is the successive step performed after a reaction network is defined; hence, it is not the scope of the current study.

The reaction environment of the synthesis solutions was varied by conducting reactions in two solvent systems, under air and inert atmospheres, and by using two boron reducing agents that have different reduction rates. The observations provide evidence for several important reaction processes that control initial Au^I : phosphine complexes, grow metal cores, and modify core nuclearity. We use PSEP theoretical analyses^{10–12} and apply the isolobal analogy^{28–32} to help account for the reaction intermediates and products. Comparisons among the results of this and previous studies provide evidence that the gold-diphosphine systems are governed by disparate reaction pathways from different growth platforms (defined as the stable lower nuclearity cluster that resists etching and allows promotion of growth).²⁴ For the current Au : L⁵ system, the growth platforms are cationic clusters that form immediately after the addition of the reducing agent. In the absence of L⁵, reduction of the [Au^I(PPh₃)₂]⁺ precursor complex results in the almost total extinguishment of all ionic signals, indicating the initial Au : ligand complex distribution affects which reduction and nucleation pathways predominate. These results identify a need for more research to better understand the role of different ligands during cluster formation.

Experimental methods

The current study uses UV-vis and ESI-MS to monitor the distribution of [Au_{*x*}L_{*y*}(PPh₃)_{*w*}]^{*z*+} clusters. To the eye, nearly all phosphine ligated Au_{*x*} : 2 ≤ *x* ≤ 13 clusters display color, and their spectra exhibit distinct, broad absorption bands between 250 nm and 650 nm.^{3,11,24,33–36} Conductivity and ESI-MS studies have established that stable, phosphine-ligated Au_{*x*} : 2 ≤ *x* ≤ 13 clusters carry positive charge; a finding that is also predicted by PSEP theory.^{5,22,26,33–35,37–42}

Synthesis, storage, and analysis operations were conducted at ambient temperature ($T = 21$ °C to 24 °C). All chemicals and solvents were purchased from Sigma-Aldrich and used as delivered.⁴³ The MPC synthesis solutions used during these experiments are similar to those reported previously.^{14,24} Briefly, Au(PPh₃)Cl (99.9+%), L⁵, and a reducing reagent, borane *tert*-butylamine complex (BTBC, 97%) or NaBH₄ (≥ 99%), were weighed out in a 1 : 1 : 5 molar ratio, and dissolved in either 1 : 1 methanol : chloroform or neat (100%) chloroform to give [Au(PPh₃)Cl] = 5.0 × 10^{−3} mol L^{−1}. Cluster stability can change as function of solvent system.⁴⁴ These reaction conditions produced the greatest number of observed ionic species. We determined the optimum reducing agent to Au(PPh₃)Cl ratio by observing the threshold, where additional NaBH₄ induced the appearance of (NaB(OCH₃)₄)_{*n*}^{*z*+}

polymers, observed for $>1200 m/z$, and $[\text{Na}^+ \text{CH}_3\text{O}]_x$ clusters, observed for $<800 m/z$.⁴⁵

Deaerated synthesis solutions were prepared in a 20 mL borosilicate glass, crimp-sealed vial into which solvent, $\text{Au}(\text{PPh}_3)\text{Cl}$, and L^5 were added. While the solution was being mixed with a magnetic stirbar, argon was bubbled through it to minimize the presence of dissolved gases. (Vial components and stirbars were never reused.) After the mixture of ligand complexes equilibrated (≈ 15 min.),⁴⁶ dry reducing agent (BTBC or NaBH_4) was quickly added (defining $t = 0$ min), the solution was again purged with argon, and the vial was crimp sealed. During these last operations the solution was temporarily stagnant. To minimize the introduction of oxygen, a syringe was used to remove samples through the septum.

To observe the effects of oxygen, a set of aerated syntheses were also conducted. The aerated syntheses were prepared in open containers and covered to prevent evaporation losses, but stirred in the presence of air; therefore, we will refer to solutions prepared with this procedure as aerated syntheses.

As the reactions progressed, small samples were collected and diluted in methanol for analysis either by UV-vis or ESI-MS (in $10\times$ to $10\,000\times$ dilution). Samples were analyzed within ≈ 5 min of their dilution. UV-vis spectra of aerated solutions were collected on a Varian Cary II dual beam spectrometer.

ESI-MS data were obtained in negative and positive ion modes. The mass spectrometer comprised an electrospray ion source (Analytica of Branford), coupled to a custom-built (by Ardra Technologies) Extrel CMS quadrupole mass spectrometer (mass range $\approx 10 m/z$ to $\approx 3000 m/z$). Samples were introduced to the ESI source *via* direct infusion ($10 \mu\text{L min}^{-1}$) through a glass capillary. The source was purged with ≥ 1.0 mL of methanol between samples. The source electrical potentials, temperature, curtain gas flow, and effusion rate were optimized to maximize ion intensities while minimizing fragmentation. Stable ion currents and the spectra presented here were obtained with the potential difference between the capillary exit and the skimmer set to 80 V; however, to assure data quality and consistency, additional spectra were systematically collected for voltages between 60 V and 140 V.

Dynamic light scattering (DLS) measurements were conducted using a Malvern Zetasizer Nano ZS equipped with a 4 mW 633 nm laser. Since domain-induced scattering within 1:1 methanol:chloroform solution corrupts measurements, DLS measurements were conducted on synthesis solutions prepared in 1:1 methanol:diethyl ether (Sigma Aldrich, CHROMASOLV, 99.9%, inhibitor free).⁴⁷ Prior to the addition of the precursor reagents, the methanol was passed through a $0.2 \mu\text{m}$ filter to remove dust. The competing product from the methanol: NaBH_4 reaction produced precipitate that was removed by centrifugation at $\approx 1 \times 10^5 \text{ m s}^{-2}$ (10 kg_n) for 30 min. In addition, DLS measurements were conducted on solutions containing dissolved ligands, $\text{Au}(\text{PPh}_3)\text{Cl}$ alone, NaBH_4 alone, and dissolved NaBH_4 and ligands together; these measurements exhibited null results, increasing the acceptance that the DLS distributions derived for reaction solutions correlate to $[\text{Au}_x\text{L}^5_y]^{z+}$ containing colloid formation only.

Results

A. Au_x cluster growth with BTBC

Fig. 2a shows the distribution of solution complexes that form with equimolar concentrations of $\text{Au}(\text{PPh}_3)\text{Cl}$ and L^5 in deaerated 1:1 methanol:chloroform. The ESI-MS ion signal is dominated by $[\text{Au}_2\text{L}^5_2]^{2+}$. The spectrum shows much weaker signals from $[\text{Au}(\text{PPh}_3)_2]^+$, $[\text{Au}(\text{PPh}_3)\text{L}^5]^+$, $[\text{AuL}^5_2]^{2+}$, and trace signal from $[\text{Au}_2\text{L}^5_2\text{Cl}]^+$.

The reduction reaction is initiated by the addition of 5 X molar excess BTBC to the equimolar $\text{Au}(\text{PPh}_3)\text{Cl}:\text{L}^5$ 1:1 methanol:chloroform solutions (Fig. 2). At $t = 5$ min, the ESI-MS spectrum exhibits trace signals from $[\text{Au}_8(\text{PPh}_3)\text{L}^5_3]^{2+}$ and $[\text{Au}_8\text{L}^5_4]^{2+}$ (inset of Fig. 2a). In negative ion mode ESI-MS data exhibited only Cl^- in unreduced and reduced solutions.

After BTBC is added, the solution gradually changes color from clear to light brown to orange to dark red, and it finally develops a dark colloid by $t = 1.5$ h. For comparison, in solutions containing only $\text{Au}(\text{PPh}_3)\text{Cl}$ that are reduced by 5 X molar excess BTBC the black colloidal suspension develops by $t = 30$ min. This result indicates that the presence of L^5 changes the rate of reduction.

With increasing time the ESI-MS data exhibit an emergence of new ionic products. At $t = 1$ h, (Fig. 2b) the data exhibit new products: $[\text{Au}_{10}(\text{PPh}_3)\text{L}^5_4]^{2+}$ and $[\text{Au}_{10}\text{L}^5_4]^{2+}$. The relative signal intensities of the ionic clusters appear to be similar to or greater than the initial complexes with the $[\text{Au}_8\text{L}^5_4]^{2+}$ and $[\text{Au}_{10}\text{L}^5_4]^{2+}$ products exhibiting the strongest signal intensities.

By $t = 78$ h (Fig. 2c), the ESI-MS data show signal from $[\text{Au}_{11}\text{L}^5_5\text{Cl}]^{2+}$, $[\text{Au}_{10}\text{L}^5_4(-\text{L}^5)]^{2+}$, and $[\text{Au}_{12}(\text{PPh}_3)\text{L}^5_3(-\text{L}^5)_3\text{Cl}]^{3+}$, where $-\text{L}^5$ denotes monodentate complexation. In some cases presence of a monodentate $-\text{L}^5$ ligand can be confirmed by covalent labeling of the free phosphine terminus with oxygen. A trace of free oxygen is admitted into the sample vial, which oxidizes the free phosphine terminus, forming the monodentate $-\text{L}^5\text{O}$ ligand, where $-\text{L}^5\text{O} = 1$ -diphenyl-5-diphenylphosphine oxide pentane, *cf.* Fig. 1. At 78 h ESI-MS signals observed from $[\text{Au}_{10}\text{L}^5_4(-\text{L}^5\text{O})]^{2+}$ and $[\text{AuL}^5(-\text{L}^5\text{O})]^+$ (Fig. 2c) identify the monodentate $-\text{L}^5$ structures in the parent species.

At $t = 9$ days (Fig. 2d), ESI-MS signals representing larger nuclearity clusters emerge. Signal from $[\text{Au}_{12}(\text{PPh}_3)\text{L}^5_3(-\text{L}^5\text{O})_3\text{Cl}]^{3+}$, confirms the structure of the $[\text{Au}_{12}(\text{PPh}_3)\text{L}^5_3(-\text{L}^5)_3\text{Cl}]^{3+}$ cation. Interestingly, the signal from $[\text{Au}_{11}\text{L}^5_5\text{Cl}]^{2+}$ is fully depleted, and the signal intensity of $[\text{Au}_8\text{L}^5_4]^{2+}$ is diminished relative to the ligated Au_{10} clusters. The solution complex, $\text{Au}(\text{PPh}_3)_2^+$, is also depleted, and the relative intensity of $[\text{Au}_2\text{L}^5_2]^{2+}$ is decreased.

At $t = 77$ days ESI-MS data show increased ion intensities from larger nuclearity clusters (Fig. 2e). The ESI-MS data evince signal from $[\text{Au}_{11}\text{L}^5_4\text{Cl}]^{2+}$, $[\text{Au}_{11}(\text{PPh}_3)\text{L}^5_4\text{Cl}]^{2+}$, $[\text{Au}_{11}\text{L}^5_5\text{Cl}]^{2+}$, $[\text{Au}_{12}\text{L}^5_5\text{Cl}_2]^{2+}$, and $[\text{Au}_{12}\text{L}^5_6\text{Cl}_2]^{2+}$. We determined that $[\text{Au}_{12}\text{L}^5_6\text{Cl}_2]^{2+}$ has the structure, $[\text{Au}_{12}\text{L}^5_3(-\text{L}^5)_3\text{Cl}_2]^{2+}$, by observing trace ESI-MS signal from the covalently labeled $[\text{Au}_{12}\text{L}^5_3(-\text{L}^5\text{O})_3\text{Cl}_2]^{2+}$ (not annotated in Fig. 2e), which confirms the $-\text{L}^5$ count. ESI-MS signal from $[\text{Au}_{11}\text{L}^5_5\text{Cl}]^{2+}$ has reappeared, mostly in its oxidized form, $[\text{Au}_{11}\text{L}^5_4(-\text{L}^5\text{O})\text{Cl}]^{2+}$, which also reveals one $-\text{L}^5$. The $[\text{Au}_8\text{L}^5_4]^{2+}$ signal is depleted, as are signals from $[\text{Au}_{12}(\text{PPh}_3)\text{L}^5_3(-\text{L}^5)_3\text{Cl}]^{3+}$ and $[\text{AuL}^5]^+$. The depletion of signal from Au_8 clusters is

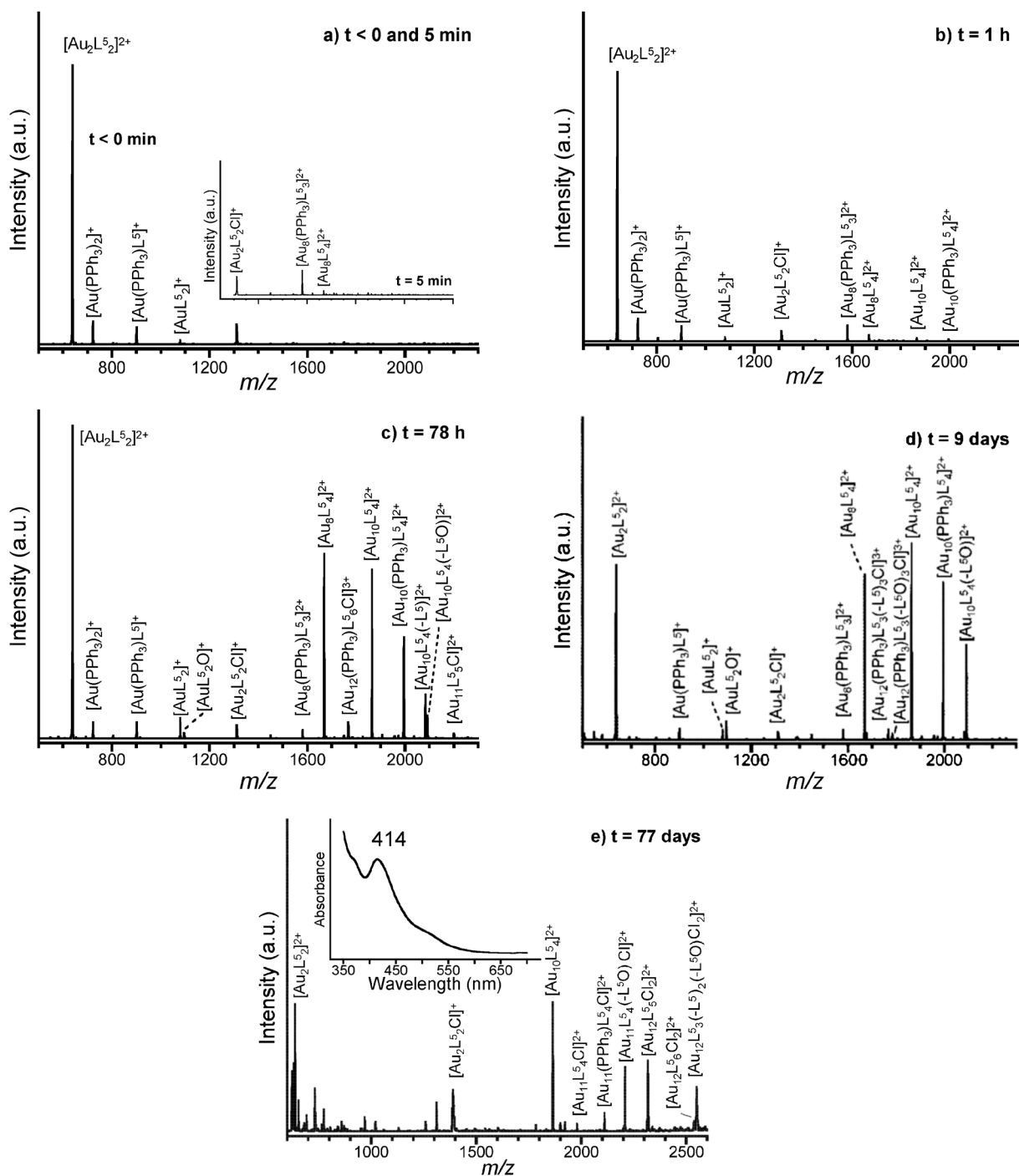


Fig. 2 ESI-MS spectra of deaerated, 1 : 1 methanol : chloroform solutions, prepared with 1 : 1 molar ratio of L^5 and $Au(PPh_3)Cl$, observed at (a) $t < 0$ min, solution complexes prior to initiation of reduction (inset shows $t = 5$ min after BTBC addition); (b) $t = 1$ h; (c) $t = 78$ h; (d) $t = 9$ days and (e) $t = 77$ days after the addition of 5 X molar ratio BTBC (Inset: UV-vis spectrum of the synthesis solution at $t = 77$ days. Absorptions at $\lambda_{max} = 414$ nm and the shoulder near 367 nm are features characteristic of $\{Au_{11}, Au_{12}\}$ and Au_4 , respectively. The weak absorption between $\lambda = 480$ nm to 540 nm ($\lambda_{max} \approx 510$ nm or 520 nm) originates from agglomerations of primary clusters. See text.).

indicative of their reactive nature in the synthesis solution. The corresponding UV-vis spectrum (inset of 2e) displays a blue shifted absorption band centered at 414 nm, indicating a shift of the product distribution to larger gold nuclearity.⁴⁸

The UV-vis spectrum also exhibits a weak absorption band centered between 510 nm and 520 nm that is consistent with the signature of agglomerated primary clusters.^{14,49} In accord

with this assignment, addition of excess L^5 (relative to initial $Au(PPh_3)Cl$) extinguishes this absorption band, indicating that the agglomerated primary clusters are resorbed into solution, as they are transformed into more stable species.¹⁴ Since the resulting UV-vis spectrum is little changed, the data suggest that the size distribution of the resorbed primary clusters is similar to that of the nascent solution species.

These species may include neutral clusters due to the distribution of complexes being reduced.

The evolution of the transient and final product distributions observed with ESI-MS is similar for the methanol:chloroform and pure chloroform solvent systems; however, product formation in the pure chloroform is faster. Fig. S1 shows the product formation from $t = 5$ min to $t = 9$ days.† Similar to the methanol:chloroform syntheses at $t \approx 5$ min, ESI-MS data exhibit $[\text{Au}_8(\text{PPh}_3)\text{L}^5_3]^{2+}$ and $[\text{Au}_8\text{L}^5_4]^{2+}$ signals (Fig. S1a†). Signals from $[\text{Au}_{10}(\text{PPh}_3)\text{L}^5_4]^{2+}$, $[\text{Au}_{10}\text{L}^5_4]^{2+}$, $[\text{Au}_{10}\text{L}^5_4(-\text{L}^5)]^{2+}$, $[\text{Au}_{11}\text{L}^5_5\text{Cl}]^{2+}$ and $[\text{Au}_{12}(\text{PPh}_3)\text{L}^5_3(-\text{L}^5)_3\text{Cl}]^{3+}$ are observed at $t = 1$ h (Fig. S1b†). The relative ion current intensities of products to initial complexes are much greater in pure chloroform, as compared to the methanol:chloroform syntheses at similar time points. During product formation up to $t = 9$ days, the relative signal intensities of $[\text{Au}_8\text{L}^5_4]^{2+}$ and $[\text{Au}_2\text{L}^5_2]^{2+}$ diminish as corresponding growth is observed among the ligated Au_{10} , Au_{11} and Au_{12} clusters. Clusters containing $(-\text{L}^5\text{O})$ also accompany these species (Fig. S1d†). In both pure chloroform and methanol:chloroform syntheses, signals from Au_6 , Au_7 or Au_9 species are not observed in the ESI-MS and UV-vis data. Overall, similar product formation and distributions are observed in both solvent systems.

When compared with deaerated methanol:chloroform syntheses initiated with BTBC, ESI-MS data observed at early time points in aerated solutions generally show a similar sequential emergence of increasing cationic cluster nuclearity. At $t \approx 5$ min $[\text{Au}_8(\text{PPh}_3)\text{L}^5_3]^{2+}$ is clearly observed (Fig. S2a†), followed by the emergence of $[\text{Au}_8\text{L}^5_4]^{2+}$ and $[\text{Au}_6\text{L}^5_3]^{2+}$ species at $t = 30$ min (Fig. S2b†). The $[\text{Au}_6\text{L}^5_3]^{2+}$ peak persists in aerated solutions for the duration of the experiment. By $t = 8$ h (Fig. S2c†), ESI-MS signal from $[\text{Au}_9\text{L}^5_4]^{3+}$ appears and grows in intensity over the subsequent seven days (Fig. S2d and e†). As the reaction progresses, $[\text{Au}(\text{PPh}_3)_2]^+$ and $[\text{Au}(\text{PPh}_3)\text{L}^5]^+$ are depleted, but $[\text{AuL}^5_2]^+$ is only slightly diminished; this result indicates that the reduction rate of $[\text{AuL}^5_2]^+$ is slower than for PPh_3 containing complexes. ESI-MS data for these aerated solutions do not exhibit signal from higher nuclearity clusters nor from any cluster containing a Cl^- ligand.

The aerated and deaerated ESI-MS data show the full depletion of ligated Au_8 clusters with increasing time, providing corroborating evidence for their reactive nature. However, the fate of the ligated Au_8 clusters is difficult to determine through comparisons of the fractional ion intensities. Ligated Au_{10} cluster signals do not increase with the depletion of the ligated Au_8 clusters (Fig. S2†), as was observed for the deaerated systems (Fig. 2), which limits the ability to follow transient products in aerated systems beyond $t = 24$ h. Overall, the aerated systems produce distinct clusters, *e.g.*, $[\text{Au}_9\text{L}^5_4]^{3+}$ and $[\text{Au}_6\text{L}^5_3]^{2+}$, that appear before $t = 8$ h, and these species remain present for the entire time period monitored. After synthesis initiation with BTBC, $[\text{Au}_8(\text{PPh}_3)\text{L}^5_3]^{2+}$ and $[\text{Au}_8\text{L}^5_4]^{2+}$ are the earliest ionic clusters observed in both deaerated and aerated systems, indicating a limiting role for the oxidative environment during nucleation and core growth.

The synchronous UV-vis spectra provide temporal sampling of the cationic and neutral cluster distributions for almost all Au_x : $x \leq 13$ clusters, allowing comparison of the total

distribution to the cationic species present in the ESI-MS data at early time points. Fig. S3 shows the accumulated, temporally resolved UV-vis spectra of a stirred, aerated synthesis solution that is reduced with BTBC in 1:1 methanol:chloroform.† The spectra show that the 420 nm band is present almost immediately ($t \leq 5$ min), and by $t \approx 1$ h, the synthesis solutions exhibit a broad molecular absorbance band centered at $\lambda_{\text{max}} \approx 420$ nm. After $t = 24$ h, the UV-vis spectra of the reaction solution remain relatively unchanged for the remaining duration of the experiment. The decreasing rate in reduction promotes an environment containing similar reaction rates for growth and degradation through oxidation.

Timed, UV-vis spectra of aerated solutions that are reduced by BTBC (Fig. S3†) exhibit neither the dark appearance of agglomerates nor the weak UV-vis absorption band that evidences agglomerates. ESI-MS data for the aerated solutions are absent of Cl^- containing clusters. The absence of both agglomeration peaks in UV-vis and Cl^- -containing clusters in the ESI-MS suggests that oxidative degradation can serve as a deagglomeration agent.

In summary, deaerated methanol:chloroform reaction solutions reduced with BTBC initially produce ligated Au_8 and Au_{10} clusters. The ESI-MS signal from ligated Au_8 clusters is depleted by $t = 77$ days, and the fractional ion intensity of the ligated Au_{10} clusters is proportionately increased. During this same time period ligated Au_{11} and Au_{12} clusters emerge (Fig. 2e). Similar formation and degradation products are observed in both solvent systems with the rate of processing occurring faster in pure chloroform. By $t = 77$ days both the ESI-MS and UV-vis data report a shift of the cluster distribution to higher gold nuclearity. The UV-vis spectra show that clusters form almost immediately and that the growth of cluster absorption bands is significant within a few hours after BTBC addition.

The ESI-MS total ion signal in deaerated systems shows a proportionate transfer of total ion signal from low nuclearity complexes, *e.g.*, $[\text{Au}_2\text{L}^5_2]^{2+}$, to higher nuclearity clusters, *e.g.*, ligated Au_8 and Au_{10} . Evolution of the ESI-MS data indicate that $[\text{Au}_8(\text{PPh}_3)\text{L}^5_3]^{2+}$ forms before or simultaneously with $[\text{Au}_8\text{L}^5_4]^{2+}$, that $[\text{Au}_8\text{L}^5_4]^{2+}$ forms before the Au_{10} cations (*e.g.*, $[\text{Au}_{10}\text{L}^5_4]^{2+}$, $[\text{Au}_{10}(\text{PPh}_3)\text{L}^5_4]^{2+}$, and $[\text{Au}_{10}\text{L}^5_4(-\text{L}^5)]^{2+}$), and that the ligated, cationic Au_8 species are consumed to depletion in deaerated MPC syntheses. Finally, in aerated solutions, the formation of ligated $[\text{Au}_6\text{L}^5_3]^{2+}$ and $[\text{Au}_9\text{L}^5_4]^{3+}$ is observed promptly at $t \approx 0.5$ h and $t = 8$ h, respectively.

B. Au_x cluster growth with NaBH_4

We conducted deaerated experiments with NaBH_4 to observe the effects of a faster reducing agent upon $\text{Au}:\text{L}^5$ syntheses in methanol:chloroform solutions. Prior to reaction initiation, a similar complex distribution observed in the BTBC syntheses is measured (Fig. 2a). Again, reduction was initiated by adding 5 X molar excess NaBH_4 . Immediately, the solution turned dark brown in color, forming colloids of agglomerated primary clusters.¹⁴ During the next 30 min, the solution developed a distinct reddish tint and decreased turbidity. The corresponding absorption band is observed in the UV-vis spectrum at $\lambda_{\text{max}} = 420$ nm. The absorption band at 420 nm is

characteristic of ligated Au_8 and Au_{10} clusters,²⁴ and its intensity correlates with signal intensities observed by ESI-MS among the ionic products.

Fig. 3a shows the ESI-MS spectrum twenty minutes after NaBH_4 addition. ESI-MS signal from the initial complexes: $[\text{Au}_2\text{L}^5_2]^{2+}$, $[\text{Au}(\text{PPh}_3)\text{L}^5]^+$, $[\text{Au}(\text{PPh}_3)_2]^+$, and $[\text{AuL}^5_2]^+$ are depleted or greatly diminished. These signals are replaced by abundant ESI-MS signal from $[\text{Au}_8\text{L}^5_4]^{2+}$, $[\text{Au}_{10}\text{L}^5_4]^{2+}$, $[\text{Au}_{10}(\text{PPh}_3)\text{L}^5_4]^{2+}$, and $[\text{Au}_{10}\text{L}^5_4(-\text{L}^5)]^{2+}$. Notably, signal from $[\text{Au}_8(\text{PPh}_3)\text{L}^5_3]^{2+}$ is absent. The rapid depletion of the $[\text{Au}_2\text{L}^5_2]^{2+}$ species likely allows cluster formation to be dominated by condensation reactions among fully or partially reduced digold complexes.

At $t = 67$ days, ESI-MS signals from $[\text{Au}_8\text{L}^5_4]^{2+}$, $[\text{Au}_{10}\text{L}^5_4]^{2+}$, and $[\text{Au}_{10}(\text{PPh}_3)\text{L}^5_4]^{2+}$ persist along with oxidized $[\text{Au}_{12}(\text{PPh}_3)\text{L}^5_3(-\text{L}^5\text{O})_3\text{Cl}]^{3+}$ and $[\text{Au}_{10}\text{L}^5_4(-\text{L}^5\text{O})]^{2+}$ (Fig. 3b). It is at this time that $[\text{Au}_8(\text{PPh}_3)\text{L}^5_3]^{2+}$ is first observed. Reappearance of $[\text{Au}_2\text{L}^5_2]^{2+}$ and $[\text{Au}(\text{PPh}_3)_2]^+$ in the ESI-MS spectra is observed, which suggests that less stable

clusters have been etched back into solution,¹⁴ and the resulting gold complexes become partitioned between $[\text{Au}_2\text{L}^5_2]^{2+}$ and $[\text{Au}(\text{PPh}_3)_2]^+$, in accord with solution equilibrium. Signals from $[\text{Au}_6\text{L}^5_3]^{2+}$ and $[\text{Au}_9\text{L}^5_4]^{2+}$ are absent, which is consistent among all deaerated syntheses. In contrast to the BTBC initiated syntheses, solutions reduced by NaBH_4 , do not exhibit ligated Au_{11} and Au_{12} clusters.

The UV-vis spectrum at $t = 67$ days (Fig. 3b inset) exhibits an absorption maximum, $\lambda_{\text{max}} \approx 417$ nm, that is red-shifted relative to the corresponding λ_{max} observed in synthesis solutions reduced with BTBC. The ESI-MS data show the absence of larger nuclearity clusters built from the ligated Au_{10} platform, thus, accounting for the red-shift. The weak absorption, centered at $\lambda_{\text{max}} \approx 500$ nm, fits the UV-vis absorption signature observed for solutions containing agglomerated primary clusters.³

Dynamic light scattering experiments demonstrate that the L^5 ligand exercises strong control on colloidal size distribution. As previously reported, the reduction of a 1 : 1 methanol : diethyl ether solution of $\text{Au}(\text{PPh}_3)\text{Cl}$ by NaBH_4 (in the absence of L^3 or L^5) produces colloids of agglomerated primary clusters within 5 min.¹⁴ The DLS data find that the colloids have a wide distribution of mean diameters (Fig. S4†). However, subsequent addition of 3 X molar excess L^5 to the $\text{Au}(\text{PPh}_3)\text{Cl}$ product rapidly narrows the size distribution to $D_h \approx 100$ nm in < 10 min, indicating the ability of L^5 to exert strong control on the product distribution *via* solution processing. We note that the identification of chemical species present during nucleation with a gold-phosphine precursor is currently an active area of research.⁵⁰

Discussion

A. Active reaction classes during syntheses

During these studies, the synchronously measured UV-vis and ESI-MS data support the development of the (partial) reaction network that governs L^5 -protected cluster formation in methanol and methanol : chloroform mixtures. We accomplish this goal by identifying transient and final clusters present in the reaction network and then associate these species with reaction pathways. Identifying the reaction network with relative rate information (—most importantly identifying whether specific channels are active or not—) allows a roadmap to be developed for the possible products that can be selectively produced.

The data reveal important features about the reaction network. First, the rapid growth of the absorption band centered near 420 nm indicates that most of the ligated Au_8 and Au_{10} cores form quickly. Second, the growth of ESI-MS signal, corresponding to ligated Au_8 and Au_{10} cores, appears to track the growth of the 420 nm UV-VIS signal; consequently, we conclude that the majority of nascent, ligated Au_8 and Au_{10} clusters form as cations. This result differs greatly from the reduction of monogold complexes, where efficient reduction of the gold complex distribution yields mostly neutral, ligated Au_x clusters.^{14,45} Third, the end products of BTBC and NaBH_4 syntheses differ. In syntheses reduced by NaBH_4 , the relative signal intensities of the nascent ligated Au_8 and Au_{10} clusters are preserved for long periods of time ($t > 67$ days).

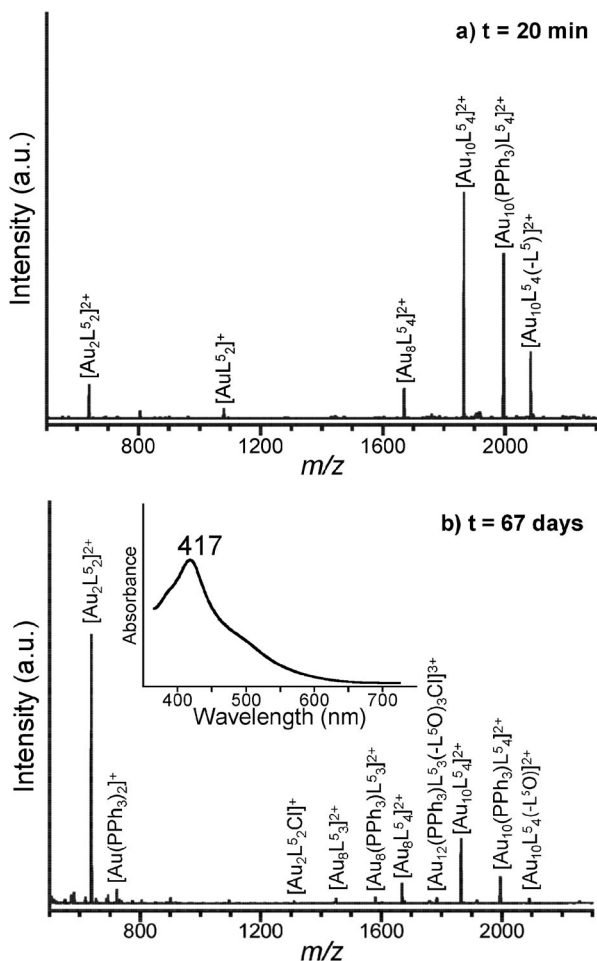
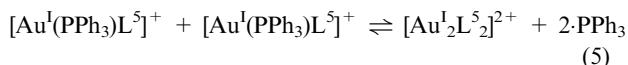
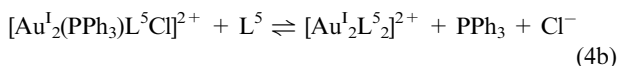
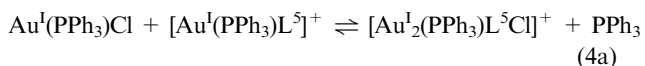
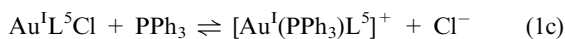
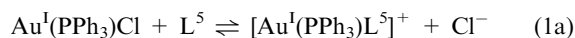


Fig. 3 ESI-MS spectra of a stirred, deaerated solution, prepared with 1 : 1 molar ratio of L^5 and $\text{Au}(\text{PPh}_3)\text{Cl}$ in 1 : 1 methanol : chloroform, observed at a) $t = 20$ min and b) $t = 67$ days after the addition of 5 X molar ratio NaBH_4 (Inset: Associated UV-vis absorption spectrum exhibiting $\lambda_{\text{max}} = 417$ nm and a shoulder centered near 365 nm. The weak absorption, centered at $\lambda_{\text{max}} = 500$ nm, originates from agglomerations of primary clusters. See text.)

In contrast, the cluster evolution during BTBC syntheses shows continued growth from ligated Au₈ to Au₁₀ species, followed by the appearance of larger ligated Au₁₁ and Au₁₂ clusters. Finally, syntheses conducted in aerated systems yield unique gold nuclearity clusters.

Discussion of the reaction classes and corresponding reaction pathways are presented. Since the present study is insensitive to clusters of $m/z > 3000$ in the ESI-MS and to neutral clusters of Au_x: $13 < x < 25$ in the UV-vis data, this survey of the reacting species is likely incomplete; however, the presently observed species serve as sign-posts along the synthetic path from initial reactants to larger product clusters.

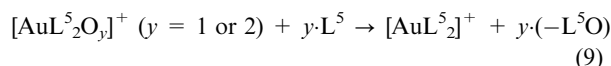
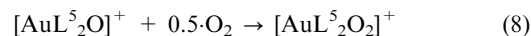
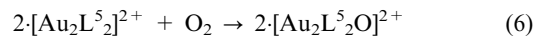
(1) Ligand-exchange induced dissolution of Au^I(PPh₃)Cl. Dissolution of Au^I(PPh₃)Cl to ionic species determines the distribution of Au:ligand complexes present prior to reduction. Bergeron *et al.* have previously proposed a set reactions that produce monogold, two-coordinate complexes;⁵¹ however, the current data are dominated by reactions involving the digold complex, [Au₂L⁵₂]²⁺, so dissolution to form an equilibrated solution likely proceeds *via* the following reactions:



Reactions (1) through (5) account for the majority of complexes observed by ESI-MS in equilibrated solutions. This reaction scheme is incomplete, as the equilibria include chlorinated-complexes and likely other ternary and quaternary phosphine containing complexes. Other dimeric Au(PPh₃)Cl species have been predicted to be stable species by maximizing dipole interactions;⁵² therefore, ligand exchange with these dimeric species is predicted to occur at higher concentrations of L⁵. Above, we treat [Au₂L⁵₂]²⁺ and [Au₂L⁵₂Cl]⁺ as species stabilized by bridging L⁵ ligands, which is in accord with the structure of [Au₂L⁵₂]²⁺ (L⁵ = bis(diphenylphosphino)methane).³⁸ We only treat Au^IL⁵Cl as a transient intermediate that is not present (and not reduced) in equilibrated solutions.

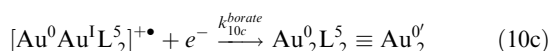
The complexes present in solution are susceptible to oxidation when stirred in ambient conditions. Bergeron *et al.*⁵¹ previously demonstrated *via* ESI-MS that [AuL⁵₂]⁺ was the salient feature observed at [L⁵]/[Au(PPh₃)Cl] = 12 in aerated, pure chloroform solvent systems. Experiments conducted under argon in deaerated solutions of neat CHCl₃ without reducing agents show that the formation and persistence of

[Au₂L⁵₂]²⁺ species is consistent with the initial solution complex distributions in methanol:chloroform mixtures (Fig. 2a). When the vial is open to air, oxidation of the complexes is readily observable, indicating an oxidation degradation pathway for the [Au₂L⁵₂]²⁺ complex to [AuL⁵₂]⁺ that occurs quickly. These data are consistent with the reaction sequence:



Additional data are needed to confirm this reaction sequence; however, the reaction scheme predicts the formation of [AuL⁵₂]⁺, which putatively promotes the production of the observed ligated Au₉ cores in stirred, aerated synthesis solutions under ambient conditions (Fig. S2†). In contrast, stirred, deaerated synthesis solutions do not form cationic [Au₉L_xO_y]^{z+} clusters at any time in synthesis solutions, and they do not promote the increasing formation of [AuL⁵₂]⁺ (Fig. 2 and 3, S1 and S2†). See supporting information for more complete details on the stability of complexes and clusters in aerated solutions.

(2) Reduction of [Au^ILL]⁺ and [Au^I₂L⁵₂]²⁺ to form reduced gold species. In the current study, we provide evidence for disparate reduction rates and reduction efficiencies of complexes containing PPh₃ and fully exchanged L⁵-containing complexes. Solution-phase reduction of complexes is symbolized as:



where Au^I is a gold complex cation (*e.g.*, [Au(PPh₃)₂]⁺, [Au(PPh₃)L⁵]⁺ and [AuL⁵₂]⁺), Au⁰₂ is a reduced, ligated Au species (*e.g.*, Au⁰₂L⁵₂), Au⁰Au^I is a free radical gold species with 0.5 reduction efficiency (*e.g.*, [Au⁰Au^IL⁵₂]^{+\bullet}). The electron is donated by the borane reducing agent, BTBC or NaBH₄;^{53–55} L, L' = (PPh₃, L⁵); and k_{10}^{borate} is the global reduction rate of the specified gold species for the reducing reagent solution. Prior work on the reduction of Au^I species in solution has reported that the alcohol radical manifests insufficient potential to promote formation of Au⁰;⁵⁶ therefore, the reduction is dependent on the availability of the boron reducing agent (BTBC or NaBH₄). For simplicity, we define Au⁰ to denote a generalized Au⁰LL'• free radical and Au⁰Au^I to denote the [Au⁰Au^IL⁵₂]^{+\bullet} free radical cation, so that we may present subsequent reactions without explicitly accounting for the ligands on the gold reactants and products.

Important factors controlling product formation related to the reduction process with boron include: (i) the relative rate

of reduction for NaBH₄ and BTBC in solvent systems and (ii) the efficiency of the reduction process, *i.e.*, the percentage of Au^I conversion in a complex to Au⁰. The reaction with NaBH₄ and methanol has a reported half-life $t_{1/2} < 0.5$ h,⁵³ therefore, because Au^I reduction occurs rapidly and the characteristic signal from the methanol-NaBH₄ is absent in ESI-MS spectra, the reduction rate of the gold complexes is equal to or greater than the NaBH₄ reaction with methanol. By comparison, the relative reduction rates of Au^I solution complexes by BTBC are slower than by NaBH₄, indicating a longer lifetime of the BTBC reducing environment. The change in the reducing rate observed for Au(PPh₃)Cl *vs.* Au(PPh₃)Cl:L⁵ solutions, reduced by BTBC provides evidence for disparate rates of reduction for each solution complex.

For the current system, the complex distribution is dominated by [Au₂L⁵]²⁺ (Fig. 2a). As captured by reactions (10b) and (10c), the immediate transfer of ionic character from complexes to cluster products in solutions reduced by NaBH₄ suggests that reduction efficiency drives the nascent cluster distribution. Recombination reactions among fully (reaction (10c)) and partially reduced (reaction (10b)) complexes result in cationic cluster formation. These reactions account for the predominance of L⁵-ligated Au₁₀ clusters at early time for solutions reduced by NaBH₄ (Fig. 3).

The present and a prior study⁵¹ show the persistence of [AuL⁵]⁺ in the ESI-MS data, indicating that this complex is much less reactive. The diminished reactivity could arise if solution phase [AuL⁵]⁺ is a complex and the reduction intermediates comprise ternary and quaternary gold-phosphine borohydride complexes (formed by attachment of a borohydride ligand). Fully chelated [AuL⁵]⁺ would be expected to react more slowly than unchelated complexes, [Au(PPh₃)₂]⁺ and [Au(PPh₃)L⁵]⁺. Regardless of the mechanism, the greater reduction rates observed for [Au(PPh₃)₂]⁺ and [Au(PPh₃)L⁵]⁺ suggest that nascent MPCs should contain both PPh₃ and L⁵ ligands, especially in syntheses initiated by BTBC.

(3) Nucleation and core growth of ligated Au_x clusters.

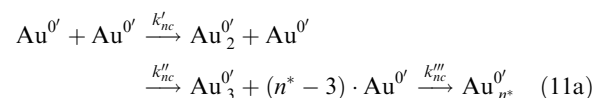
Cluster formation occurs through two distinct stages. Stage 1 comprises reduction and nucleation, and stage 2 comprises the subsequent solution phase processing. The rate and duration of reduction will control the amount of overlap between the stages. For this work the initial formation (stage 1) of gold nanoclusters is illustrated with a classical nucleation model because no current experimental setup can track individual species during reduction and nucleation events.

Theoretical results indicate that the classical model can serve as a mathematical approximation of the actual chemical reaction network leading to ligated Au₇ clusters. Evans and Mingos⁵⁷ have shown that the binding for ligated gold clusters of the form, [Au–PPh₃]_n; 2 ≤ n ≤ 6, can be described by the hy(s – z) orbitals of the Au–PPh₃ fragments. X-ray crystallography and ¹⁹⁷Au Mössbauer and ³¹P{¹H} NMR spectroscopy of [Au₇(PPh₃)₇]⁺ find that the [Au–PPh₃]_n structural form extends to n = 7.¹ Since the Au–PPh₃ fragment is isolobal to [Au⁰(PPh₃)₂][•],^{30,48,57} we hypothesize that [Au⁰(PPh₃)₂][•] self-reaction and reactions of [Au⁰(PPh₃)₂][•] with other (Au–PPh₃)_n (n < 8) clusters will have low barriers to condensation.³⁰ Alternately, Guidez *et al.*⁵⁰ have also proposed a set of stable

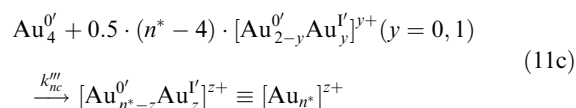
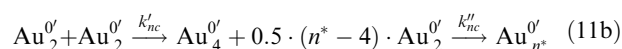
phosphine-protected gold clusters, Au_x; x ≤ 4, built from the Au(PPh₃)Cl precursor. Although these kinetically driven condensation reactions allow the formation of higher energy, metastable species, the more active fraction of the reaction network will comprise low energy pathways that can be predicted by consideration of the isolobal principle. Thus, the chemical reaction network that generates low nuclearity clusters can be approximated by fitting data with a classical nucleation model. The model itself provides insight into the growth process.

The distribution of complexes resulting from equimolar concentration of Au(PPh₃)Cl and L⁵ is dominated by bridging, digold clusters, *e.g.*, [Au₂L⁵]²⁺. Two nucleation models are incorporated to account for the immediate formation of stable, neutral and cationic clusters above the critical nucleus, n*, where dΔG^o/dn = 0. ΔG^o is the Gibb's reaction energy for the addition of an atom to the ligated Au_n cluster.¹⁸ Importantly, the nucleation models are dependent upon the recombination reactions of free radical complexes; hence, the nucleation rates are driven by the reduction rates of Au^I species (reactions (10)).

Nucleation Model 1 (reduced [Au^ILL']⁺ complexes):



Nucleation Model 2 (reduced [Au^I₂L⁵]²⁺ complexes):



where z specifies the number of [Au⁰Au^IL⁵]⁺ added during the reaction sequence indicated in reaction (11c). For Nucleation Model 1 and Model 2 particle growth data can be characterized with the global nucleation reaction rate coefficient, k_{nc}. Note, the nascent nucleation products reflect both the metal atom count and the nature of the phosphine ligand complexation. The presence of both mono- and digold complexes likely portends that both nucleation models will be active and weighted by the distribution of complexes present.

For the present synthesis experiments involving slower reduction by BTBC, it is possible that a significant fraction of the Au_x ensemble may never reach the critical nucleus size n*; therefore, product yield may diminish. However, for synthesis experiments involving rapid reduction by NaBH₄, which yields immediate formation of predominately cationic clusters, we presume Nucleation Model 2 should dominate. The immediate formation of ligated, cationic Au₈ and Au₁₀ clusters induced by reduction with NaBH₄ indicates reduction efficiencies of less than 1 for the digold complexes. This is also consistent with previously reported cationic cluster formation through the rapid reduction of [Au₂L⁶]²⁺.²⁴

ESI-MS spectra from BTBC syntheses show the initial formation of [Au₈(PPh₃)L⁵]²⁺ (Fig. 2, S1, and S2[†]), which is

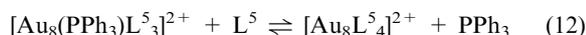
consistent with the PPh₃-containing complexes being preferentially reduced (or having an increased reduction rate compared to the [Au₂L⁵₂]²⁺ complexes). Therefore, in BTBC syntheses the initial formation of Au_x clusters obtains contributions from both nucleation models.

Both nucleation models contain reaction paths leading to the formation of neutral clusters. For example, for a solution that is rapidly reduced by NaBH₄ (or BTBC) at early times the abrupt elevated concentration of neutral complexes may rapidly react, for instance, through the sequence of reactions (11a) involving [Au⁰LL'][•] (L, L' = PPh₃, L⁵) and reactions (11b) involving Au⁰₂L⁵₂, yielding a distribution of neutral Au_wL_xL'_y: w ≥ n* clusters. In the present experiments with solutions reduced by BTBC the formation of neutral species is supported by the increased reduction rate of the PPh₃-containing complexes that follow Nucleation Model 1. Although neutrals have a certain probability of forming, the predominance of ionic complexes, e.g., [Au⁰Au^IL⁵₂]^{•+}, increases the likelihood that reaction (11c) will interpose into the reaction sequence, thus, converting the neutrals into cationic clusters.

The ESI-MS spectra of the NaBH₄ syntheses do not immediately exhibit [Au₈(PPh₃)L⁵₃]²⁺. This absence is expected when cluster formation is dominated by the reduction of [Au₂L⁵₂]²⁺. Although [Au^I(PPh₃)_nL⁵_{2-n}]⁺ (n = 1 or 2) complexes are reduced simultaneously with [Au₂L⁵₂]²⁺, the liberation of excess L⁵ initiates fast ligand exchange on the nascent clusters, producing [Au₈L⁵₄]²⁺ from [Au₈(PPh₃)L⁵₃]²⁺. As previously stated, the relative rate of reduction for NaBH₄ is very fast; thus, all available species are rapidly reduced, which effectively eliminates the observation of preferential reduction of specific complexes. The majority of the distribution of complexes (predominantly [Au₂L⁵₂]²⁺) is reduced, and the nucleation process should be driven by Nucleation Model 2. Note, the sequential addition of Au⁰₂ and Au⁰Au^I species can be changed, but the final nucleation products will comprise the same stable, cationic clusters.

The reduction efficiency of the complexes in solution cannot be well modelled in the current system, but the proportionate transfer of ion signal intensity from complexes to yield intense signals from ligated Au₈ and Au₁₀ clusters indicates that the majority of initial products should be cationic instead of neutral, as is predicted by Nucleation Model 2. Fast product formation is consistent with observation of the corresponding ligated Au₈ and Au₁₀ ion peaks in the ESI-MS and distinct red color in solution within t = 0.5 h (inset of Fig. 3).

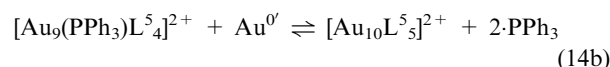
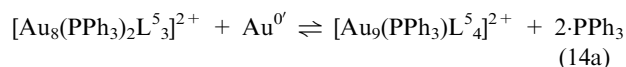
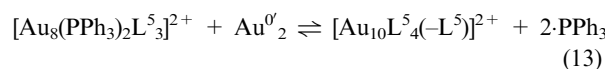
(4) Ligand exchange reactions at the Au_x core. ESI-MS data in aerated and deaerated systems show that [Au₈(PPh₃)L⁵₃]²⁺ appears prior to [Au₈L⁵₄]²⁺ during BTBC syntheses. This result evidences the activity of ligand exchange reactions among the Au₈ species, e.g.,



Ligand exchange reactions that replace PPh₃ with L⁵ are favored because L⁵ binds more strongly with gold.^{51,58} Thus, ligand exchange reactions analogous to reaction (12) are available to all gold species containing PPh₃. Although L⁵ is

a bidentate ligand, the nascent addition complex may involve monodentate complexation, which is followed by an auto-logous ligand exchange that forms a fully complexed L⁵ while displacing a PPh₃ or Cl⁻. Over time, the ligand caps of almost all Au_x species in a mixture will exchange, and the ligand cap of the end-products will predominantly contain the stronger binding ligand.

(5) Product Formation from cationic platforms. During deaerated syntheses with BTBC, ligated Au₈ cations appear first in the ESI-MS data. The subsequent appearance of ligated Au₁₀ cluster cations is evidence for core growth from the ligated Au₈ clusters. Ligated Au₁₀ can form through the addition of ligated, reduced gold species, e.g.,



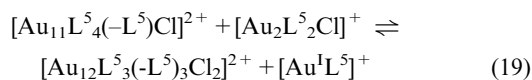
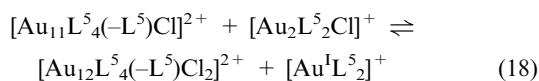
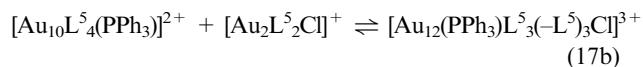
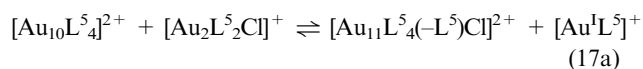
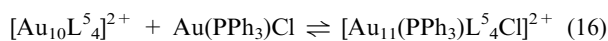
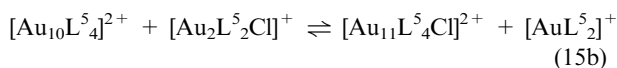
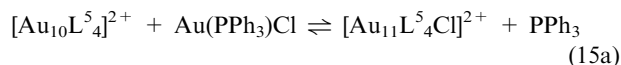
The ligands on the Au^{0'} and Au^{0'}₂ species that are not incorporated in the cluster product are predicted to be liberated into solution. Similar addition reactions involving [Au₈L⁵₄]²⁺ will also be active. Reaction (13) incorporates the addition of a fully reduced digold complex, Au^{0'}₂, which represents R₃P–Au⁰–Au⁰–PR₃ (PR₃ = PPh₃ or L⁵). We expect the substitution of L⁵ for the PPh₃ protecting ligand on the Au^{0'}₂ species will affect stability.^{50,59} Using relativistic SCF calculations, Schwerdtfeger *et al.*²⁹ have described the orbital structure of the related stable species, PH₃–Au⁰–Au⁰–PH₃.

Reaction (14) is an alternative pathway to the formation of ligated Au₁₀ clusters. The mechanism involves a sequence of reactions that add Au^{0'} to Au₈ and Au₉ species. However, the ESI-MS data show no evidence for Au₉ clusters. The absence of ligated Au₉ signals indicates that reaction (14) is essentially inactive. Therefore, based on the predicted stability of the Au^{0'}₂ and on the absence of Au₉ clusters, we conclude that reaction (13) depicts the dominant pathway to [Au₁₀L⁵₅]²⁺. The absence of ligated Au₉ clusters due to digold addition (reaction (13)) is consistent with previously observed formation pathways with L⁶-protected Au₈ clusters that form [Au₁₀L⁶_y]²⁺.²⁴

When considering the total number of valence electrons in a cluster (n_{ve}), PSEP theory predicts that stable, phosphine-protected, gold centered clusters have their peripheral gold atoms in toroidal (n_{ve} = (12n_s + 16)e⁻) or spherical (n_{ve} = (12n_s + 18)e⁻) arrangements, where n_s is the number of skeletal electrons donated by the peripheral gold atoms.^{3,10,57} PSEP analyses of [Au₈(PPh₃)L⁵₃]²⁺ and [Au₈(PPh₃)₂L⁵₃]²⁺ find total valence electron counts (each Au, P, and Cl⁻ correspondingly contributes 11, 2 and 1 valence electrons) of 100 e⁻ and 102 e⁻, which cause their peripheral gold atoms to lie in toroidal and spherical arrangements, respectively. [Au₁₀L⁵₄(-L⁵)]²⁺, [Au₁₀(PPh₃)L⁵₄]²⁺, and [Au₁₀L⁵₄(-L⁵O)]²⁺ each contains 126 e⁻ and nine peripheral gold atoms (n_s = 9); thus, each is a stable species that has its peripheral gold atoms in spherical arrangements (i.e., n_{ve} = (12n_s + 18) = 12(9) + 18 = 126 e⁻). Likewise, PSEP theory finds that

$[\text{Au}_{10}\text{L}^5_4]^{2+}$ (124 e^-), which has an uncovered gold atom, is stable with its peripheral gold atoms in a toroidal arrangement. Although $[\text{Au}_{10}\text{L}^5_4\text{L}']^{2+}$ ($\text{L}' = \text{PPh}_3, -\text{L}^5, -\text{L}^5\text{O}$) and $[\text{Au}_{10}\text{L}^5_4]^{2+}$ are observed during experiments, the predominance of $[\text{Au}_{10}\text{L}^5_4]^{2+}$ among the final products (Fig. 2e and 3b) may reflect the effects of steric hindrance within the ligand cap. The product formations can be described with the total valence e^- and topographical structures: $[\text{Au}_{11}\text{L}^5_4\text{Cl}]^{2+}$ (136 e^- , toroidal), $[\text{Au}_{11}(\text{PPh}_3)\text{L}^5_4\text{Cl}]^{2+}$ (138 e^- , spherical), $[\text{Au}_{11}\text{L}^5_4(-\text{L}^5)\text{Cl}]^{2+}$ (138 e^- , spherical), $[\text{Au}_{12}\text{L}^5_4(-\text{L}^5)\text{Cl}_2]^{2+}$ (150 e^- , spherical), $[\text{Au}_{12}\text{L}^5_3(-\text{L}^5)_3\text{Cl}]^{2+}$ (150 e^- , spherical), and $[\text{Au}_{12}(\text{PPh}_3)\text{L}^5_3(-\text{L}^5)_3\text{Cl}]^{3+}$ (150 e^- , spherical), indicating that these species can be expected to be stable and to contain a central gold atom. The accord enhances confidence in the assignment of the ESI-MS peaks.

At longer time periods during the BTBC syntheses, the formation of larger clusters is observed through the addition of $\text{Au}:\text{L}^5$ complexes to $[\text{Au}_{10}\text{L}^5_4]^{2+}$. The growth pathways can all be described through ligated gold additions, which are isolobal to the fragments in the gold-centered clusters, to the Au_{10} platform:



These ligated Au_{11} and Au_{12} clusters appear in pure chloroform solution but on much faster time scales than observed in methanol:chloroform solvent. This difference indicates that the BTBC reduction environment is more important for product formation than the solvent mixture itself. Formation pathways involving the addition of free Cl^- in solution can also be developed, but these pathways are not predicted to significantly contribute to product formation.²⁴

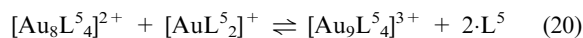
The phosphine-ligated Au_{12} clusters produced during syntheses are novel, as the ligand configurations determined by ESI-MS are those that PSEP theory predicts for gold cores containing a central gold atom. The other confirmed Au_{12} :phosphine cluster contains no central atom.⁶⁰ The preponderance of Au_{12} clusters ligated by L^5 engaged in monodentate complexation, may indicate that steric hindrance among ligands determines much of the structure.

Considerations of stabilization energy and steric hindrance can account for the reactivities observed among ligated Au_8 , Au_{10} , Au_{11} and Au_{12} clusters. PSEP theory finds that the ligated clusters appearing in the ESI-MS data are all minimum

electronic energy structures; however, steric hindrance from ligands can increase with nuclearity. Although persistent solutions of $[\text{Au}_8(\text{PPh}_3)\text{L}^5_3]^{2+}$ and $[\text{Au}_8\text{L}^5_4]^{2+}$ can be prepared, structure determinations of analogous $[\text{Au}_8(\text{PPh}_3)_n]^{2+}$ ($n = 7, 8$) clusters^{22,41} reveal metal frameworks that are wide open to $[\text{Au}_2\text{L}^5_2\text{Cl}_n]^{2+}$ ($n = 0, 1$) addition; hence, ligated Au_{10} clusters are readily prepared from Au_8 complexes. In solution, ligated Au_{10} clusters exist with an uncovered peripheral gold atom are open to addition of a gold complex (reactions (15)–(17)), forming stable, fully-ligated Au_{11} species. Although L^5 , $-\text{L}^5$, PPh_3 , and Cl^- ligands cover most of the Au_{10} or Au_{11} cores, these clusters remain available for reaction, forming ligated Au_{12} clusters (reactions (17b)–(20)).

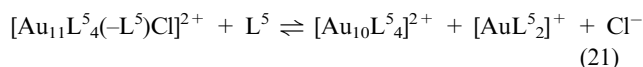
Interestingly, the syntheses do not form $\text{Au}_{13}:\text{L}^5$ clusters, which theoretically are very stable, due to a closed skeletal shell.^{10–12,37} The absence of this product may arise from steric hindrance at the crowded Au_{12} surface that blocks AuLL' and $[\text{Au}_2\text{L}^5_2\text{Cl}_n]^{2+}$ ($n = 0, 1$) addition.

(6) Etching processes. The products, $[\text{Au}_6\text{L}^5_3]^{2+}$ and $[\text{Au}_9\text{L}^5_4]^{3+}$, are unique to the aerated synthetic solutions. These products form under conditions where the oxidation of the $[\text{Au}_2\text{L}^5_2]^{2+}$ to $[\text{AuL}^5_2]^+$ is expected (reactions (6)–(9)). The formation of $[\text{Au}_9\text{L}^5_4]^{3+}$ is expected to occur through the addition of $[\text{AuL}^5_2]^+$:



With increasing time $[\text{Au}_9\text{L}^5_4]^{3+}$ grows concurrently with increasing $[\text{AuL}^5_2]^+$ concentration (Fig. S2†). More evidence is provided by the concurrent formation of $[\text{Au}_9\text{L}^5_4]^{3+}$ with the decreasing peak intensity of the $[\text{Au}_8\text{L}^5_4]^{2+}$. In aerated syntheses the formation of $[\text{Au}_6\text{L}^5_3]^{2+}$ occurs within $t = 0.5$ h after BTBC addition. Its formation may be promoted through an increased concentration of available oxygen that supports an etching process. Additional studies are ongoing to better characterize the reaction.

Evidence for etching of Au_{11} clusters is observed in deaerated solutions. Fig. 2 shows that signal from $[\text{Au}_{11}\text{L}^5_4(-\text{L}^5)\text{Cl}]^{2+}$ is depleted by $t = 9$ days. The net etching reaction likely occurs through:



The product distribution in the BTBC syntheses is likely to include some cationic clusters outside the m/z range of our instrument, indicating that other etching reactions from higher nuclearity clusters may account for the formation of some observed products.

In conclusion, ligated, cationic Au_8 and Au_{10} clusters form quickly in both solvent systems and with both reducing agents. $[\text{Au}_8\text{L}^5_4]^{2+}$ is more reactive than $[\text{Au}_{10}\text{L}^5_4]^{2+}$, as evidenced by the diminished signal of ligated Au_8 clusters in both solvents. The $[\text{Au}_{10}\text{L}^5_4]^{2+}$ cluster is a growth platform for larger nuclearity clusters forming through further addition reactions and is resistant to degradation. Solutions reduced by NaBH_4 do not form Au_{11} and only a trace of Au_{12} species, possibly indicating that the product yield for ligated Au_8 and Au_{10} clusters is higher than observed with BTBC. Finally, in aerated

syntheses unique product formation is observed that is attributed to the oxidation of the initial complexes.

B. Comparison of $\text{Au}_x:\text{L}^3$ and $\text{Au}_x:\text{L}^5$ cluster formation

We recently examined the reaction network governing cluster formation in the $\text{Au}(\text{PPh}_3)\text{Cl}:\text{L}^3$ system with similar experimental protocol.⁴⁵ Although the protecting diphosphine ligands are electronically similar, the reduction of complexes containing either L^3 or L^5 reacts *via* different formation and degradation pathways.

The initial complex distributions formed by equal molar additions of $\text{Au}(\text{PPh}_3)\text{Cl}$ and L^n ($n = 3$ or 5) are different, and these differences strongly influence the reduction efficiencies of the complex ensemble. For unreduced solutions that contain L^5 , mass spectra indicate that $\sim 85 \pm 10\%$ of the TIC can be attributed to complexes containing no PPh_3 . In contrast, for unreduced solutions that contain L^3 , only $\sim 55 \pm 10\%$ of the TIC is due to complexes containing no PPh_3 . This fact indicates that L^5 replaces PPh_3 more efficiently than L^3 . Furthermore, the complex distribution arising in an equimolar solution of L^5 and $\text{Au}(\text{PPh}_3)\text{Cl}$ is dominated by digold complexes, whereas the distribution in the $\text{Au}(\text{PPh}_3)\text{Cl}:\text{L}^3$ solution is dominated by monogold complexes. Critically, these complexes are the starting materials for the reduction and nucleation reactions that lead to cluster formation. Thus, the tendency of the digold complexes to degrade to monogold complexes *via* oxidation under ambient conditions is of special interest.

The initial complex distribution determines which nucleation model is applicable to cluster formation after reduction.⁶¹ ESI-MS data indicate differences in the reduction rate of the ligated Au^{I} species as a function of protecting ligands and coordination number. In systems reduced with BTBC, complexes containing PPh_3 are always diminished prior to the complexes that contain exclusively L^n ($n = 3$ or 5) (Fig. 2, S1 and S2[†]). Although the reduction of complexes containing L^n is expected, the relative reduction rates are slower. For BTBC syntheses the slower reduction rates of the $[\text{Au}_2\text{L}^n_2\text{Cl}_y]^{(2-y)+}$ ($y = 0$ or 1) species result in the nucleation process being initially dominated by the free radical recombination of $\text{Au}^0\text{LL}'^{\bullet}$ (Nucleation Model 1). Because the equimolar L^5 system has much less initial monogold complexes, its contribution of neutral nucleation products is expected to be limited, and nucleation products should be controlled by Nucleation Model 2, which forms cationic clusters. Similarly, the equimolar L^3 systems consist of more PPh_3 -containing complexes, and the subsequent nucleation products are predominantly neutral clusters formed *via* Nucleation Model 1. Another contributing factor in the L^3 system governed by nucleation model 1 is that the reduction efficiency of $[\text{Au}_x\text{L}^3_x]^{x+}$ is 1; whereas, a significant portion of $[\text{Au}_2\text{L}^5_2]^{2+}$ has a reduction efficiency less than 1.

The contrasting formation of ionic and neutral nucleation products for L^5 and L^3 , respectively, is enhanced in syntheses reduced with NaBH_4 , where preferential reduction is minimized by the fast reduction rate. For L^5 syntheses, cationic Au_8 and Au_{10} clusters form immediately and persist for the duration of the experiment. The persistence of the ligated Au_8 and Au_{10}

clusters likely arises from the dynamic processing of growth and etching reactions, defined as size-selective processing.¹⁴ In contrast, the almost complete reduction of the L^3 complex ensemble by NaBH_4 does not significantly increase ESI-MS cluster signal intensities; instead, the dark colloidal suspension mainly comprises neutral species, which are observed with UV-vis spectroscopy and DLS.

The nucleation product distribution and inherent properties of each diphosphine ligand contribute to the disparate final products observed in the two studies. For L^5 , few reaction pathways are observed after cessation of nucleation, but growth to the larger nuclearity clusters builds from the $[\text{Au}_{10}\text{L}^5_4]^{2+}$ cluster platform. Precedence for growth platforms is reported from Pettibone and Hudgens,²⁴ where L^6 -protected Au clusters grow from the $[\text{Au}_8\text{L}^6_4]^{2+}$ platform. The growth from $[\text{Au}_{10}\text{L}^5_4]^{2+}$ is observed and subsequent product formation is described in reactions (15)–(19).

When comparing the number and type of active reactions that form ligated clusters, the reaction network involving L^3 is more complicated. The initial neutral clusters, which are the principal nucleation products in the L^3 system, are converted to ionic species through cationic addition reactions. Simultaneously, ligand exchange reactions are prevalent because phosphine ligands are liberated into solution after nucleation. Ligand exchange of PPh_3 with L^3 on the surface of ligated Au_8 and Au_9 clusters can promote etching reactions to form $[\text{Au}_6\text{L}^3_4]^{2+}$.^{2,14} In summary, the initial formation of cationic reduction products controls the nucleation process much more tightly in L^5 syntheses than in L^3 syntheses, thus limiting the number of subsequent reactions that can occur to form the most thermodynamically stable products.

Although the L^3 and L^5 syntheses produce dissimilar final gold nuclearity clusters in deaerated systems, syntheses conducted under aerated conditions produce a distribution of overlapping cluster nuclearity. The oxidation of $[\text{Au}_2\text{L}^5_2]^{2+}$ produces increased concentration of $[\text{AuL}^5_2]^+$ (reactions (6)–(9)), which promotes the formation of $[\text{Au}_9\text{L}^5_4]^{3+}$ (reaction (20)). The presence of oxidative species also promotes the formation of $[\text{Au}_6\text{L}^5_3]^{2+}$. Both $[\text{Au}_9\text{L}^5_4]^{3+}$ and $[\text{Au}_6\text{L}^5_3]^{2+}$ are analogous to observed products in the $\text{Au}:\text{L}^3$ systems.

Conclusions

We have used UV-vis spectroscopy and ESI-MS to elucidate the active reaction network during syntheses of gold nano-clusters. The data provide evidence for the activity of different chemical reaction classes that form the solution complexes, that grow the metal cores, and that remodel core nuclearity, culminating in the formation of stable MPCs. Unlike L^3 syntheses, L^5 protected cluster formation proceeds predominantly through the initial formation of cationic species with only small contributions from neutral clusters. Thus, these properties limit the size of the active reaction network. The immediate formation of cationic MPCs is preserved in deaerated solutions with the faster reducing agent, NaBH_4 . The role of the reduction and subsequent nucleation processes is controlled by the solution complex distribution. The data for syntheses of $\text{Au}:\text{L}^5$ systems evidence that the nascent reaction products ($t < 3$ days) are less dependent on the chosen reducing agent

(BTBC or NaBH₄); instead, after reduction ceases, subsequent solution phase processing provides greater control for tuning cluster nuclearity.

The production of persistent [Au₁₀L₄]²⁺ by the slower reduction rate of BTBC leads to higher nuclearity gold clusters that are built from a reaction network centered around the [Au₁₀L₄]²⁺ platform. Although [Au₁₀L₄]²⁺ production is not affected by reducing rate, the fast reduction of (nearly) the entire complex distribution with NaBH₄ restrains subsequent growth of ligated Au₁₁ and Au₁₂ clusters. The absence of further growth is due to the absence of excess gold species, which is minimized by the faster reduction rate with NaBH₄.

By using simple electron counting rules based on PSEP analysis and isolobal relationships, we have accounted for the observed reaction intermediates and final MPC products. When constructing models of MPC syntheses, counting rules can help identify candidate solution-phase reactions. Importantly, the incorporation of covalent labelling with O-containing complexes along with PSEP analyses have allowed the confident assignment of numerous peaks in the ESI-MS that would have been otherwise difficult to identify.

The role of oxidation on the product formation was more pronounced for the L⁵ syntheses, as compared to the L³ syntheses, due to the greater susceptibility of the digold complexes to oxidation. Under ambient conditions, overlapping channels are observed in the L³ and L⁵ systems, which are not active in the deaerated systems. These experiments support the previously reported relationship between initial Au : ligand complex distribution and product formation described by Pettibone and Hudgens.²⁴ Specifically, ambient conditions manipulate the complex distribution, and subsequent product formation of ligated Au₆ and Au₉ clusters is not observed in the deaerated systems. Overall, the development of the reaction network for L⁵ containing MPCs is controlled through the ligated Au₈ and Au₁₀ platforms.

Acknowledgements

JMP acknowledges the National Academy of Science's National Research Council for postdoctoral fellowships. We thank Dr Denis E. Bergeron for advice and help with experiments involving the aerated solutions.

References

- 1 J. W. A. Vandervelden, P. T. Beurskens, J. J. Bour, W. P. Bosman, J. H. Noordik, M. Kolenbrander and J. A. K. M. Buskes, *Inorg. Chem.*, 1984, **23**, 146.
- 2 J. W. A. Van der Velden, J. J. Bour, J. J. Steggerda, P. T. Beurskens, M. Roseboom and J. H. Noordik, *Inorg. Chem.*, 1982, **21**, 4321.
- 3 K. P. Hall and D. M. P. Mingos, *Prog. Inorg. Chem.*, 1984, **32**, 237.
- 4 M. McPartlin, R. Mason and L. Malatest, *J. Chem. Soc. D, Chem. Commun.*, 1969, 334.
- 5 P. L. Bellon, F. Cariati, M. Manasser, L. Naldini and M. Sansoni, *J. Chem. Soc. D, Chem. Commun.*, 1971, 1423.
- 6 B. K. Teo, X. B. Shi and H. Zhang, *J. Am. Chem. Soc.*, 1992, **114**, 2743.
- 7 G. Schmid, *Chem. Soc. Rev.*, 2008, **37**, 1909.
- 8 C. E. Briant, K. P. Hall and D. M. P. Mingos, *J. Organomet. Chem.*, 1983, **254**, C18.
- 9 D. M. P. Mingos, *J. Chem. Soc., Dalton Trans.*, 1996, 561.
- 10 R. B. King, *Inorg. Chim. Acta*, 1986, **116**, 109.

- 11 D. M. P. Mingos, *Polyhedron*, 1984, **3**, 1289.
- 12 D. M. P. Mingos, T. Slee and L. Zhenyang, *Chem. Rev.*, 1990, **90**, 383.
- 13 M. F. Bertino, Z. M. Sun, R. Zhang and L. S. Wang, *J. Phys. Chem. B*, 2006, **110**, 21416.
- 14 J. M. Pettibone and J. W. Hudgens, *ACS Nano*, 2011, **5**, 2989.
- 15 Y. Shichibu and K. Konishi, *Small*, 2010, **6**, 1216.
- 16 G. H. Woehrl, M. G. Warner and J. E. Hutchison, *J. Phys. Chem. B*, 2002, **106**, 9979.
- 17 Y. Yanagimoto, Y. Negishi, H. Fujihara and T. Tsukuda, *J. Phys. Chem. B*, 2006, **110**, 11611.
- 18 E. E. Finney and R. G. Finke, *J. Colloid Interface Sci.*, 2008, **317**, 351.
- 19 C. E. Briant, K. P. Hall and D. M. P. Mingos, *J. Chem. Soc., Chem. Commun.*, 1984, 290.
- 20 C. E. Briant, K. P. Hall, A. C. Wheeler and D. M. P. Mingos, *J. Chem. Soc., Chem. Commun.*, 1984, 248.
- 21 R. Jin, H. Qian, Z. Wu, Y. Zhu, M. Zhu, A. Mohanty and N. Garg, *J. Phys. Chem. Lett.*, 2010, 2903.
- 22 M. Manasser, L. Naldini and M. Sansoni, *J. Chem. Soc., Chem. Commun.*, 1979, 385.
- 23 J. W. A. van der Velden, J. J. Bour, W. P. Bosman and J. H. Noordik, *Inorg. Chem.*, 1983, **22**, 1913.
- 24 J. M. Pettibone and J. W. Hudgens, *J. Phys. Chem. Lett.*, 2010, **1**, 2536.
- 25 S. Hong, G. Shafai, M. Bertino and T. S. Rahman, *J. Phys. Chem. C*, 2011, **115**, 14478.
- 26 J. W. A. van der Velden, F. A. Vollenbroek, J. J. Bour, P. T. Beurskens, J. M. M. Smits and W. P. Bosman, *Recl. Trav. Chim. Pays-Bas*, 1981, **100**, 148.
- 27 F. A. Vollenbroek, J. J. Bour and J. W. A. Vandervelden, *Recl. Trav. Chim. Pays-Bas*, 1980, **99**, 137.
- 28 D. M. P. Mingos, *Pure Appl. Chem.*, 1991, **63**, 807.
- 29 P. Schwerdtfeger and P. D. W. Boyd, *Inorg. Chem.*, 1992, **31**, 327.
- 30 M. Elian, M. M. L. Chen, D. M. P. Mingos and R. Hoffmann, *Inorg. Chem.*, 1976, **15**, 1148.
- 31 R. Hoffmann, *Angew. Chem., Int. Ed. Engl.*, 1982, **21**, 711.
- 32 D. M. P. Mingos, *Pure Appl. Chem.*, 1980, **52**, 705.
- 33 D. Li, C. M. Che, S. M. Peng, S. T. Liu, Z. Y. Zhou and T. C. W. Mak, *J. Chem. Soc., Dalton Trans.*, 1993, 189.
- 34 F. Wen, U. Englert, B. Guttrath and U. Simon, *Eur. J. Inorg. Chem.*, 2008, 106.
- 35 V. W. W. Yam, T. F. Lai and C. M. Che, *J. Chem. Soc., Dalton Trans.*, 1990, 3747.
- 36 D. P. Zhang, J. M. Dou, D. C. Li and D. Q. Wang, *J. Coord. Chem.*, 2007, **60**, 825.
- 37 C. E. Briant, B. R. C. Theobald, J. W. White, L. K. Bell, D. M. P. Mingos and A. J. Welch, *J. Chem. Soc., Chem. Commun.*, 1981, 201.
- 38 L. C. Porter, N. I. Khan, C. King and J. P. Fackler, *Acta Cryst.*, 1989, **45**, 947.
- 39 M. Schulz-Dobrick and M. Jansen, *Z. Anorg. Allg. Chem.*, 2007, **633**, 2326.
- 40 J. M. M. Smits, J. J. Bour, F. A. Vollenbroek and P. T. Beurskens, *J. Crystallogr. Spectrosc. Res.*, 1983, **13**, 355.
- 41 J. W. A. van der Velden, J. J. Bour, W. P. Bosman and J. H. Noordik, *J. Chem. Soc., Chem. Commun.*, 1981, 1218.
- 42 E. Zeller, H. Beruda and H. Schmidbaur, *Inorg. Chem.*, 1993, **32**, 3203.
- 43 Certain commercial materials and equipment are identified in this paper in order to adequately specify the experimental procedure. Such identification neither implies recommendation or endorsement by the National Institute of Standards and Technology nor does it imply that the material or equipment identified is the best available for the purpose.
- 44 O. Toikkanen, S. Carlsson, A. Dass, G. Ronnholm, N. Kalkkinen and B. M. Quinn, *J. Phys. Chem. Lett.*, 2010, **1**, 32.
- 45 J. W. Hudgens, J. M. Pettibone, T. P. Senftle and R. N. Bratton, *Inorg. Chem.*, 2011, **50**, 10178.
- 46 The equilibration time of 15 min was determined from a set of ESI-MS measurements. Au(PPh₃)Cl and L³ were added to solvent, stirred, and small samples were withdrawn for ESI-MS analyses. For the reagent weights and solvent volumes used, the ratio of ion abundances ceased to vary before 15 min passed. Thus, samples were allowed at least 15 min to equilibrate.

-
- 47 Inhibitor free diethyl ether was chosen to avoid chemical effects of the inhibitor, BHT (2,6-di-*tert*-butyl-4-methylphenol), upon syntheses and their optical measurements. Those attempting to repeat this work should keep in mind that pure, uninhibited diethyl ether is prone to forming the contact explosive, diethyl ether peroxide. Furthermore, diethylether is extremely flammable, and its autoignition temperature of 170 °C enables it to ignite without the presence of an open flame.
- 48 K. P. Hall, D. I. Gilmour and D. M. P. Mingos, *J. Organomet. Chem.*, 1984, **268**, 275.
- 49 IUPAC. Compendium of Chemical Terminology, 2nd ed. (the "Gold Book"). Compiled by A. D. McNaught and A. Wilkinson. Blackwell Scientific Publications, Oxford (1997). XML on-line corrected version: <http://goldbook.iupac.org> (2006-) created by M. Nic, J. Jirat, B. Kosata; updates compiled by A. Jenkins. ISBN 0-9678550-9-8, DOI: 10.1351/goldbook.
- 50 E. B. Guidez, A. Hadley and C. M. Aikens, *J. Phys. Chem. C*, 2011, **115**, 6305.
- 51 D. E. Bergeron, O. Coskuner, J. W. Hudgens and C. A. Gonzalez, *J. Phys. Chem. C*, 2008, **112**, 12308.
- 52 P. Schwerdtfeger, H. L. Hermann and H. Schmidbaur, *Inorg. Chem.*, 2003, **42**, 1334.
- 53 R. E. Davis and J. A. Gottbrath, *J. Am. Chem. Soc.*, 1962, **84**, 895.
- 54 H. C. Brown, E. J. Mead and C. J. Shoaf, *J. Am. Chem. Soc.*, 1956, **78**, 3616.
- 55 C. T. F. Lo, K. Karan and B. R. Davis, *Ind. Eng. Chem. Res.*, 2007, **46**, 5478.
- 56 J. Majimel, D. Bacinello, E. Durand, F. Vallee and M. Treguer-Delapierre, *Langmuir*, 2008, **24**, 4289.
- 57 D. G. Evans and D. M. P. Mingos, *J. Organomet. Chem.*, 1982, **232**, 171.
- 58 D. E. Bergeron and J. W. Hudgens, *J. Phys. Chem. C*, 2007, **111**, 8195.
- 59 J. S. Golightly, L. Gao, A. W. Castleman, D. E. Bergeron, J. W. Hudgens, R. J. Magyar and C. A. Gonzalez, *J. Phys. Chem. C*, 2007, **111**, 14625.
- 60 P. Sevilano, O. Fuhr, E. Matern and D. Fenske, *Z. Anorg. Allg. Chem.*, 2006, **632**, 735.
- 61 J. M. Pettibone and J. W. Hudgens, *Small*, DOI: 10.1002/sml.201101777.